

The Effects of Control System Stiffness Models on the Dynamic Stall Behavior of a Helicopter

Robert M. Kufeld
Aerospace Engineer
NASA Ames Research Center
Moffett Field, California

and

Wayne Johnson
Johnson Aeronautics
Palo Alto, California

Abstract

The control system stiffness of an UH-60A helicopter was measured. A description of the measurement and the results is provided. The measured control system stiffness values were used within a comprehensive analysis, CAMRAD II, to establish a baseline calculation of the rotor system during an extreme thrust condition causing dynamic stall on the rotor. The baseline CAMRAD II model is compared to measured blade shake test data and level flight, high thrust, flight test data also showing dynamic stall from the UH-60A Airloads Program to validate the baseline calculations. An evaluation of the sensitivity of the rotor system response to different control system stiffness models was made. The calculated results show that the rotor system response is significantly improved using an accurate control system model when dynamic stall is present.

Notation

b	number of blades	
c	blade chord, ft	
C_w/σ	weight coefficient,	$\frac{GW}{\pi\sigma\rho\Omega^2 R^4}$
GW	aircraft gross weight, lbs	
K	structural stiffness, ft-lbs/deg	
r	radial location, ft	
R	rotor radius, ft	
μ	advance ratio	
ρ	air density, slug/ft ³	
σ	rotor solidity, $bc/\pi R^2$	
Ω	rotor speed, rad/sec	

Presented at the American Helicopter Society 54th Annual Forum, Washington, DC, May 20-22, 1998. Copyright © 1998 by the American Helicopter Society, Inc. All rights reserved.

Introduction

Accurately predicting the dynamic stall characteristics of a helicopter rotor is one of the major goals of the rotorcraft industry. The loads caused by this condition are very important as they are used to size the helicopter control system. To accurately predict these dynamic stall characteristics, accurate models of the rotor structure, helicopter control system, linear and nonlinear aerodynamics, and inflow are required. Bousman¹ has taken a step to improve understanding of dynamic stall through a qualitative examination of UH-60A helicopter flight test data acquired during the NASA/Army UH-60A Airloads Program². One of Bousman's conclusions was that the locations of the dynamic stall events occur in a consistent pattern in terms of azimuth and radial station and is probably controlled by the torsional dynamics of the blade. A key parameter required to predict the torsional dynamics of a blade, helicopter control system stiffness, is often difficult to measure and calculate accurately. In most cases the value of the control system stiffness is only determined after flight testing when the measured value of the blade torsional frequency can be used to validate the calculations.

The control system stiffness of the UH-60A Airloads Program aircraft was measured at Ames Research Center. A description of the experimental setup and results are included within this paper. The measured control system stiffness value was used to establish a new analytical model of the rotor system. The comprehensive rotorcraft code, CAMRAD II,^{3,4} was used to calculate the baseline results of the new model for validation with flight test data collected during the NASA/Army UH-60A Airloads Program and non-rotating blade frequencies data measured in a shake test by

Hamade and Kufeld⁵. Finally, with the fidelity of the comprehensive code established, the sensitivity of blade torsional frequencies and the rotor system response during dynamic stall to different control system stiffness models was evaluated. The results indicate a moderate level of sensitivity to changes of the control system stiffness.

UH-60A Swashplate and Stationary Links

Figure 1 shows a schematic of the location of the UH-60A stationary swashplate links with respect to the rotor azimuth. The three stationary links are located unevenly around the azimuth. The three links are arranged with 90° between each of them leaving half of the swashplate unsupported for a full 180°. The UH-60A main rotor has a leading edge pitch link which, when aligned with the forward stationary link, positions the blade spindle to 90° rotor azimuth position. With the links 90° apart, the pitch links for the next two blades will also be aligned with stationary links at the 180° and 270° azimuth position.

Figure 2 shows a cut-away view of the UH-60A control system between the primary servos and the swashplate with the three stationary links labeled. Notice that the distance between the forward and lateral stationary links to the primary servos is essentially the same. However, the aft

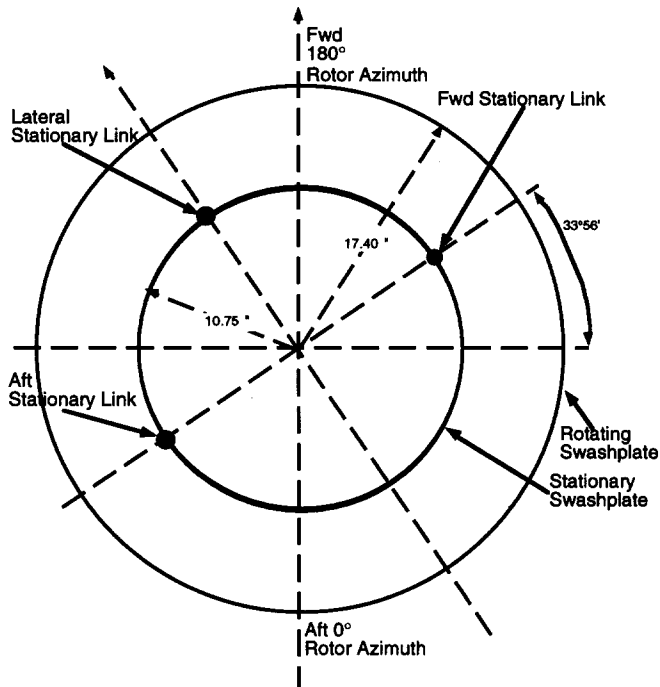


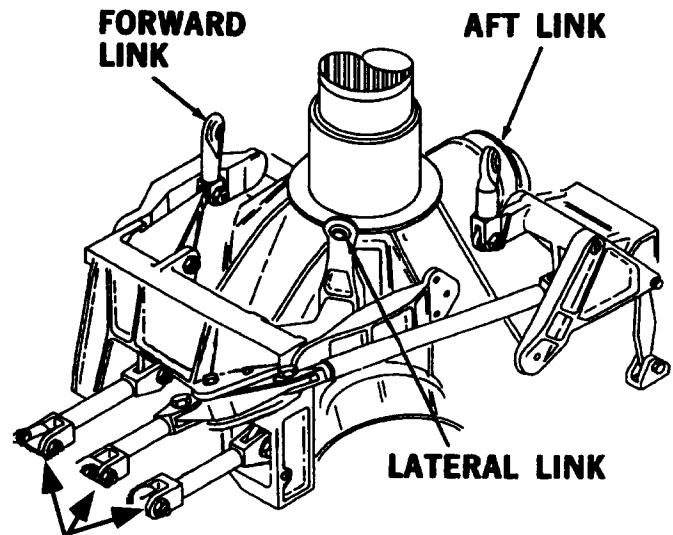
Figure 1. Schematic of the UH-60A swashplate stationary link location.

stationary link has one additional component within its series that is significantly longer than the linkages found within the other two stationary link systems.

Control Stiffness Measurement

Set-up

A measurement of the control stiffness of the UH-60A Airloads Program helicopter, tail number 748, was made at Ames Research Center. This is the same aircraft used for the NASA/Army Airloads Program. Figure 3 shows a photo of the test set up with the hardware labeled. For this test all four blades were removed and spindle adapter blocks were designed, manufactured, and installed into the blade attachment spindle using blade attachment pins. The adapter blocks served three functions. First, they served as the loading interface to the control system. A leading-edge-down pitching moment was applied to each of the four blade spindles by a six-foot moment arm attached to the adapter block. Up to 264 lbs of dead weight was applied. Secondly, the rotation of the blade spindle was measured with a 16 bit rotary encoder with a resolution of .0055 degree attached to the adapter block via a load bearing interfacing spindle. Thirdly, the adapter block was used to position the blade spindle to approximately 6° flap up and 7° lag aft to simulate the position of the blade spindle during flight. To do this the interfacing spindle was passed through a rod end



PRIMARY SERVOS CONNECTIONS

Figure 2. Cut away view of UH-60A control system linkages.

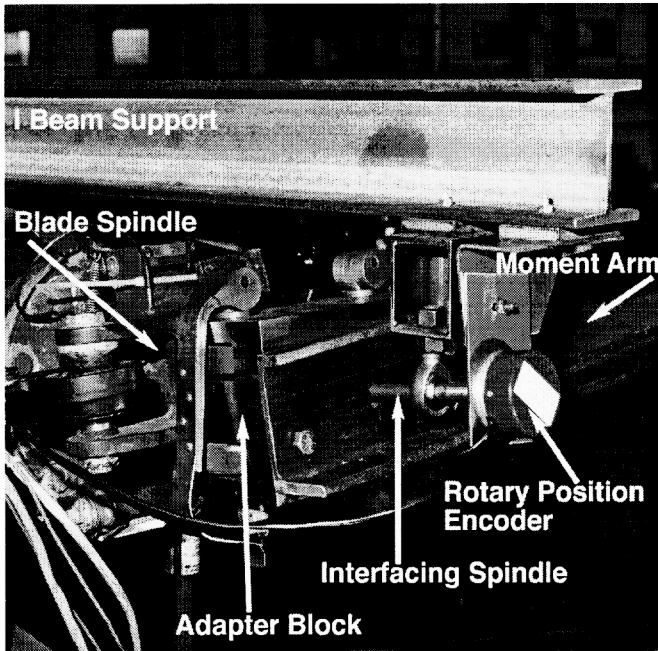


Figure 3. Photo of UH-60A blade spindle with control system stiffness hardware attached.

attached to an I-beam support structure mounted to the top of the hub. This configuration not only fixed the flap and lag position of each blade while allowing a full range of pitch motion, but also absorbed most of the vertical shear load of the dead weight and passed it along to the transmission drive shaft.

In addition to the four rotary encoders, the loads of all four pitch links were measured with strain gages and the positions of the three primary servos were measured with string potentiometers. The pitch link loads were monitored to ensure limit loads were not exceeded during loading. Any movement of the primary servos were converted to pitch deflection of the blade spindles and added to the measured spindle rotations as a correction during data processing.

Testing Procedure

The aircraft was powered with an external power unit and the aircraft's hydraulic pump was turned on to simulate normal operation during flight. To fix the controls in a repeatable position for each measurement, the flight control rigging pins were installed in all four of the control axes. Although the rigging pins allow for a fixed and repeatable position of the swashplate during each loading run, the ideal test condition -all blade

spindles at the same pitch attitude- could not be obtained because the rigged position was not at neutral cyclic. The 90° rotor azimuth position of the blade spindle was selected as the baseline position. As mentioned above this corresponds to a pitch link aligned with the forward stationary link of the stationary swashplate. Changes in azimuth positions from this baseline were measured with a transit mounted on top of the hub.

Measurements were made on all four blades simultaneously. The spindle loading was done manually with calibrated weights. The nominal load sequence started with a preload of 44 lbs, moving up to 264 lbs in 22 lbs increments, and then back down to 44 lbs, for a total of 21 measurements. This applied a maximum nose down pitching moment on the control system of 1824 ft-lbs per blade (this includes the 44 lbs preload and the weight of the moment arm, 80 lbs). Four different loading conditions were used:

1. **Collective Loading:** all four blade spindles were loaded simultaneously in the same direction from 44 to 264 lbs.
2. **Reactionless Loading:** all blades spindles started with 154 lbs load; two opposite spindles (e.g. blades at 0° & 180°) increased their loading to 264 lbs while the other set of opposite spindles (e.g. 90° & 270°) decreased their loading to 44 lbs.
3. **Cyclic Loading 1:** again starting with 154 lbs on all four blade spindles; the loading only changed on one set of opposite blades (e.g. 0° & 180°). Loading on one blade increased to 264 lbs while the loading on the opposite blade decreased to 44 lbs. The load on the 90° and 270° blade spindle remained constant.
4. **Cyclic Loading 2:** same as above, but the loading changes were performed on the other two blade spindles (e.g. 90° & 270°). The load on the 0 & 180° blade spindle remain constant.

Once a loading cycle was completed the hub was rotated 15° to a new azimuth position and the loading cycle was repeated. The loading was performed at seven different azimuth positions in all to cover the full rotation of the rotor. The first and last azimuth positions measurements provided

one set of repeated data points of a different blade spindle at the same azimuth position. (0°, 90°, 180°, 270°)

Experimental Results

After loading, the spindle angle data were corrected for movement of the primary servos and the error caused by the different angles of the blade spindles during testing. Figure 4 shows a typical example of the measured results. In most cases the blade spindle deflection has significant hysteresis, most likely caused by friction in the numerous rod ends in the control system, but the deflection usually returns to the starting value at the end of the loading. The control system stiffness of a single blade at a particular azimuth position was then approximated by the slope of a least squares curve fit to provide a linear representation of the data. It is expected that most of the hysteresis would be removed by the control system dither created in the flight environment, thus justifying a linear model.

The measured stiffnesses are unique functions of the rotor azimuth and the loading condition as is shown in Figure 5. Comparing the measured results to the physical arrangement of the UH-60A swashplate and control links (Fig. 1) improves the confidence of the measurements. As expected the largest stiffness for the collective loading mode (Fig. 5a) occurs at a blade position near 180°, where the pitch link is aligned with the lateral stationary link and the aft and forward stationary link are only 90° away. Conversely, the lowest stiffness occurs at a blade position of 360° which is the farthest point away from a stationary link.

The reactionless loading (Fig. 5b) attempts to

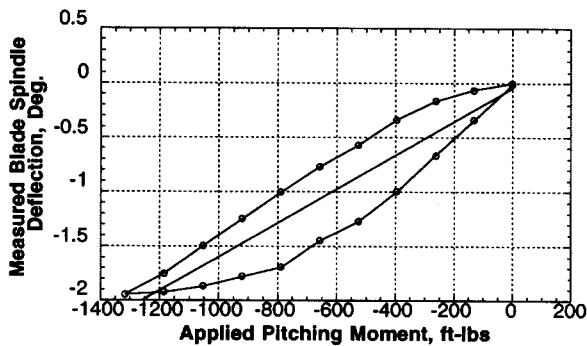


Figure 4. Typical example of loading hysteresis for collective loading of a single blade spindle; spindle at 285° azimuth.

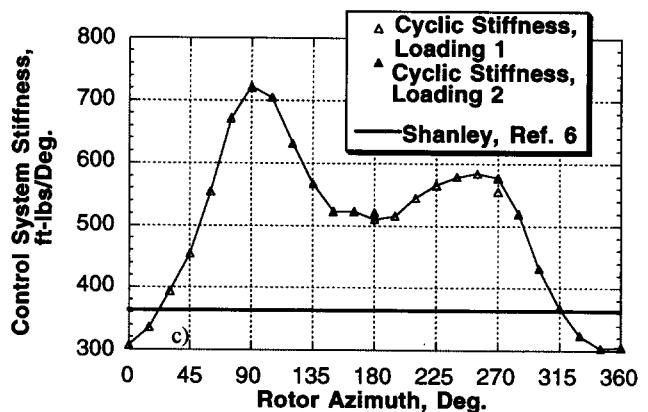
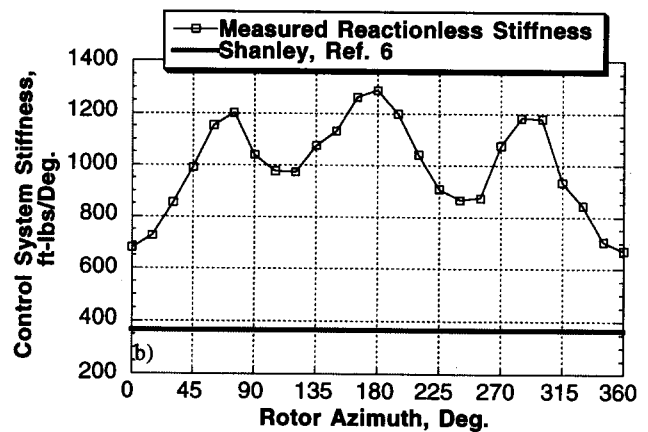
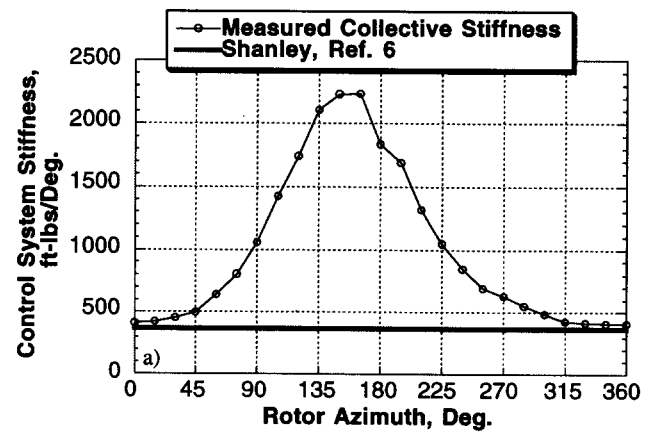


Figure 5. Measured individual blade stiffness as a function of rotor azimuth for a) collective, b) reactionless, and c) cyclic loading compared with Reference 6.

isolate the stiffness of the pitch links by keeping a constant load on the washplate and primary servos. This results in a smaller variation of stiffnesses with azimuth. The location of the primary servos is also apparent as the pitch links appears stiffer in the vicinity of the servos.

To better understand the shape of the control system stiffness due to cyclic loading (Fig. 5c) remember that the loading was done in pairs (90° & 270° and 180° & 360°). The stiffness near the 90° & 270° azimuth positions should be higher because two of the stationary links are involved while the stiffness near 180° & 360° azimuth position should be lower because only one stationary link is involved. In addition, the stiffness near 360° is much lower compared to 180° because the stationary links are far away from this azimuth position. Now refer back to Figure 2 and remember that the aft stationary link (blade spindle near the 270° rotor azimuth position) has one additional component within its linkage. This long link has the effect of reducing the stiffness near the aft link (270° azimuth) and this is seen in Figure 5c.

Also shown in Figure 5 is the published UH-60A control system stiffness from Ref. 6 (363 ft-lb/deg). This previously published value is seen to be considerably in error for all 4 loading conditions, although the published value does match the current experimental data for collective stiffness near 0° azimuth. This difference is further assessed in the results section.

Control Stiffness Model

To use the above information in the comprehensive analysis program, CAMRAD II, required the conversion of the measured control system stiffness in the rotating frame to control system stiffness in the non-rotating frame. The values were transformed using the multi-blade coordinate transformation. The equations below taken from Ref. 7 describe the transformation.

$$K_{col} = \frac{1}{N} \sum_{m=1}^N K^{(m)}$$

$$K_{cos} = \frac{2}{N} \sum_{m=1}^N K^{(m)} \cos \psi_m$$

$$K_{sin} = \frac{2}{N} \sum_{m=1}^N K^{(m)} \sin \psi_m$$

$$K_{react} = \frac{1}{N} \sum_{m=1}^N K^{(m)} (-1)^m$$

Where $K^{(m)}$ is the measured stiffness for the m th blade, ψ_m is the azimuth position of the m th blade, and N is the number of blades.

The transformation was performed for each of the four different loadings described above. Figure 6 shows the transformed values of the primary stiffness for each of the seven different azimuthal loadings. As expected, the coordinate transformation provides fixed system stiffnesses relatively independent of azimuth. As such, an average value of the stiffnesses were calculated from the seven different azimuth position measured. A (4X4) matrix shown below is the average fixed system stiffness measured during testing.

$$\begin{Bmatrix} \theta_{col} \\ \theta_{cos} \\ \theta_{sin} \\ \theta_{rea} \end{Bmatrix} = \begin{bmatrix} 897 & -135 & 57 & -32 \\ -357 & 535 & -13 & -14 \\ 128 & 1 & 698 & -53 \\ -53 & 18 & -15 & 1090 \end{bmatrix} \begin{Bmatrix} M_{col} \\ M_{cos} \\ M_{sin} \\ M_{rea} \end{Bmatrix}$$

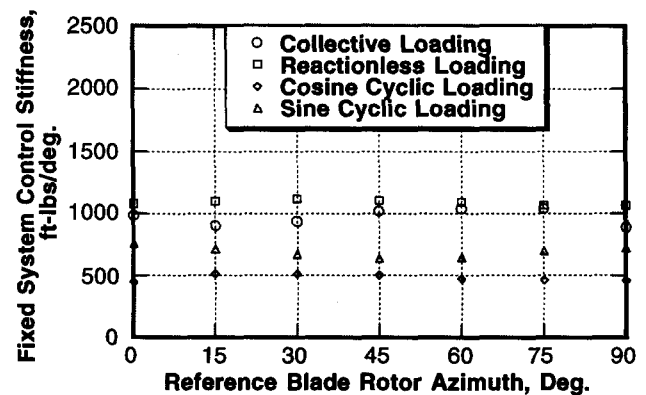


Figure 6. Diagonal elements of the fixed system control stiffness as a function of the reference blade azimuth position.

For the calculated results presented in this paper the off-diagonal terms of the fixed system control stiffness are set equal to zero. Only the diagonal terms are used to model the UH-60A control system stiffness as most comprehensive rotorcraft codes are not set-up for such a complex stiffness model.

UH-60A Math Model

The model used for the calculations performed in this paper was a modified version of the model Bousman and Maier⁸ used in an earlier study with CAMRAD/JA. The modifications include changes in format to be compatible with the CAMRAD II input format. The actual UH-60A Airloads instrumented blades were modeled. This results in minor decreases in the blade flapwise and edgewise stiffness because the pressure instrumented blade was manufactured without the nickel abrasion strip on the outboard portion of the blade. A minor change to the blade's center of gravity was made because of the instrumentation wires added to the leading edge of the blade. Lastly, a change to the aerodynamic twist of the SC1095R8 airfoil section of the blade was made to be consistent with the description of the chord line for that airfoil.

To verify the results of the new structural blade model, a comparison was made of the non-rotating blade frequencies calculated by CAMRAD II with measured shake test results⁵. Minor modifications of the CAMRAD II model enabled the calculation of non-rotating blade frequencies with the blade suspended by bungee cords from the root, very similar to the shake test configuration. Table 1 summarizes the results of this comparison.

Table 1. Comparison of measured and calculated non-rotating blade frequencies.

Blade mode	Shake Test	CAMRAD II	Per Cent Error
1st Flap	4.69 hz	4.44 hz	5.3
2nd Flap	12.46	12.60	1.1
3rd Flap	24.87	25.44	2.3
1st Chord	25.55	25.07	1.9
4th Flap	40.51	39.93	1.4
1st Torsion	44.49	46.11	3.6
5th Flap	62.28	65.52	5.2
2nd Chord	67.37	68.36	1.5

In order to accurately calculate these high frequency non-rotating modes, the blade was

modeled using eight beam elements. For rotating calculations it was sufficient to use three beam elements.

The airfoil tables used by Bousman and Maier were also slightly modified to correct for some non typical behavior within them. Lim⁹ first applied these modifications to the SC1095 airfoil deck and similar changes were made to the SC1095R8 airfoil deck used here.

Within the CAMRAD II comprehensive analysis model, the control system can be modeled with different levels of sophistication or complexity. For this study, two modeling approaches were evaluated. A simple model using only one spring for the pitch link (a rotating system representation of the control system) was evaluated first. A more complex model for the pitch link/swashplate (a fixed system representation of the control system) was also evaluated. The fixed system representation of the control system stiffness consists of four springs. A linear spring and two angular springs in the non-rotating frame, to model the collective and cyclic stiffnesses respectively of the swashplate motion, plus the above mentioned linear spring for the pitch link to model the reactionless stiffness.

One final conversion of the diagonal elements of the linearized stiffness matrix was required to obtain the proper values for the CAMRAD II model. The values of the stiffness matrix shown above were derived from measurements of the control system stiffness at the pitch bearing. The values of the spring models used within CAMRAD II require a geometric and kinematic transformation of the diagonal elements of the pitch bearing stiffness measurements to pitch link and swashplate spring values. The pitch link stiffness is a function of the measured reactionless stiffness. The swashplate collective stiffness is a function of the measured collective stiffness in series with the pitch link stiffness. The swashplate lateral stiffness is a function of measured cosine stiffness in series with the pitch link stiffness. The swashplate longitude stiffness is a function of the measured sine stiffness in series with the pitch link stiffness.

Baseline Dynamic Stall

The first objective of the CAMRAD II analysis was to correlate a baseline calculation using the rotating control system stiffness model with flight test data capturing the dynamic stall phenomenon. The second objective was to evaluate the sensitivity of the rotor response to variations in the rotating control system stiffness. Finally, the fixed system representation, four spring control system stiffness model, was inserted into CAMRAD II to evaluate the sensitivity of the rotor response.

The baseline flight test data was selected from the UH-60A Airloads Program. The Program collected a comprehensive set of level flight data points covering six different thrust coefficients, (approximately $C_w/\sigma = 0.08$ to 0.13 in 0.01 increments) within the power-limit speed boundaries of the helicopter (advance ratio between 0.0 and 0.37). From these data a set of 6 test conditions (counters) were selected to show the effects of rotor thrust at a constant value of advance ratio $= 0.23$ on the dynamic stall of this rotor system. Figure 7 shows the measured blade section pitching moment at $r/R = 0.865$ vs azimuth for each of the different thrust values. The flight pressure data shown has been decimated from a measured azimuth resolution of $\approx 1.5^\circ$ to $\approx 8^\circ$ without effecting the conclusions drawn in this paper as the CAMRAD II azimuth resolution is equal to 15° . A rapid decrease and recovery of the section pitching moment usually indicates the dynamic stall occurrence. Here two dynamic stall cycles are clearly seen at 270° and 345° azimuth for the two highest thrust conditions tested. Based on these flight data, the CAMRAD II calculation will be compared to counter 9017 with a thrust value of $C_w/\sigma = 0.13$.

For the baseline calculations the control system stiffness was modeled with a simple one spring stiffness model (rotating system representation) equivalent to the measured reactionless stiffness of 1090 ft-lb/deg. The calculations were made using the wind tunnel mode to limit comparisons to the main rotor only. A free wake and Leishman-Beddoes' dynamic stall model¹⁰ were used. The thrust and once-per-revolution flapping were trimmed to the values measured in the flight test, with the shaft angle and other operating condition variables fixed at the measured values. CAMRAD II was run to match the different level flight

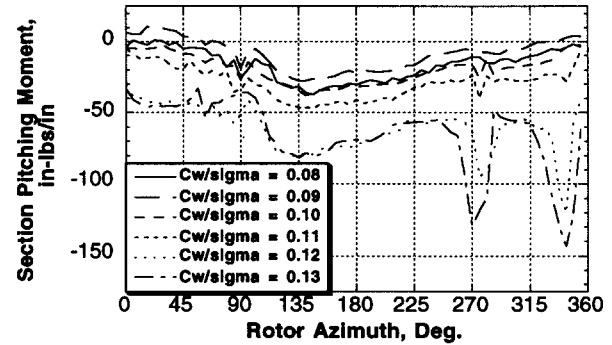


Figure 7. Measured blade section pitching moment as a function of rotor azimuth for different values of C_w/σ ; $r/R = 0.865$, $\mu = 0.23$.

conditions of $C_w/\sigma = 0.12$ and 0.13 . A summary of the results are shown in Figure 8 which compares the calculated values of blade flap bending at $r/R = 0.30$, pitch link load, and blade section pitching moment at $r/R = 0.865$ to the flight test data from counter 9017. The steady values of the structural parameters have been removed from both the calculated and flight test data to ease comparison because of poor correlation.

When comparing the calculated and measured results, the wave form of all three parameters have very similar shapes if the higher frequency content of the flight data is over looked. The predictions are sensitive to the trimmed rotor thrust. The overall magnitude of the calculated values for the pitch link load and blade section pitching moment is much lower than the measured values. The high frequency oscillations in both the pitch link load and flap bending measurements are apparently not associated with stall, since they begin in the second quadrant of the disk.

Bousman¹ showed that for this case the first stall cycles begins at around 225° azimuth on the inboard part of the blade, reaching the tip at around 290° . A major difference between the calculated and measured results is the absence of the second dynamic stall cycle present in the measured data near 340° azimuth as shown in Figure 8f.

To get better correlation for the magnitude of the oscillatory loads from the calculations, the trim procedure of the analysis was slightly changed. Additional calculations were made so that the analysis would hold a fixed collective and just trim

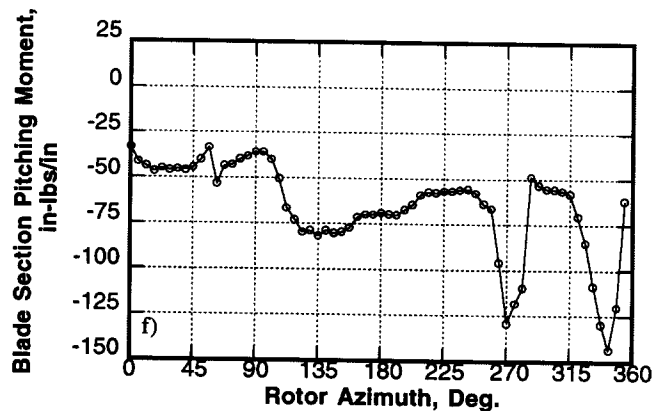
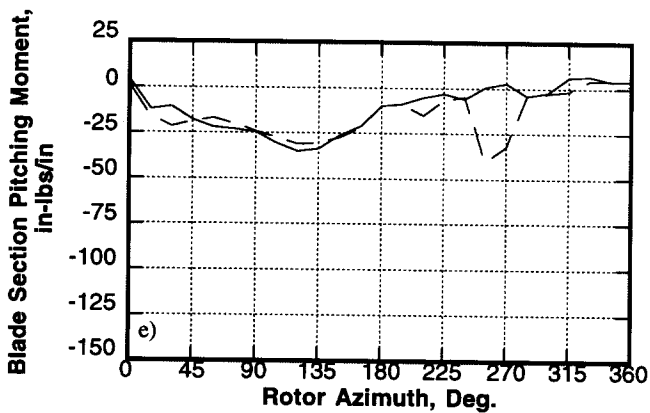
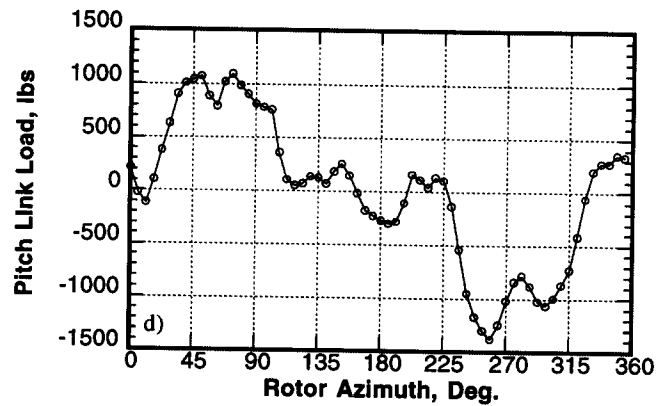
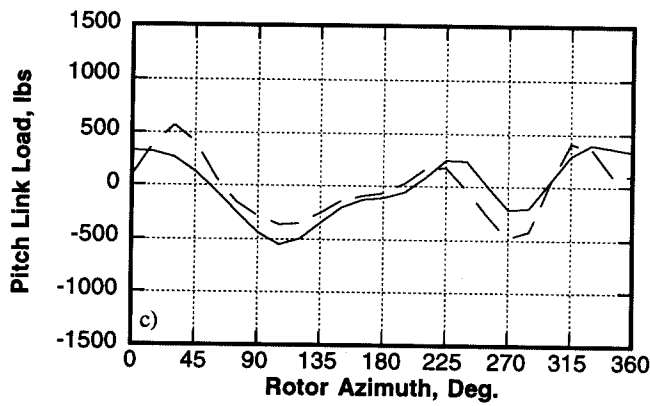
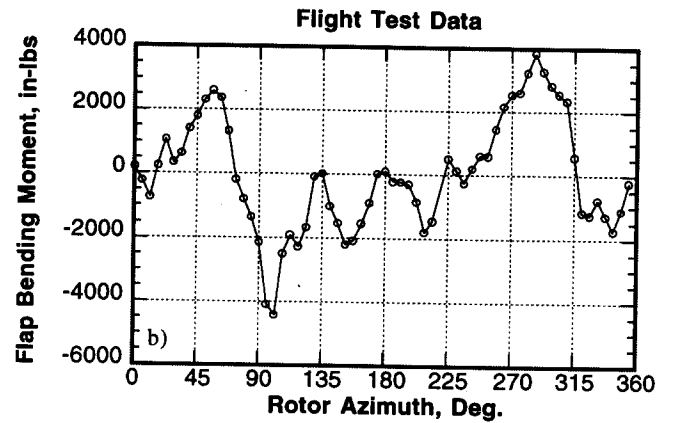
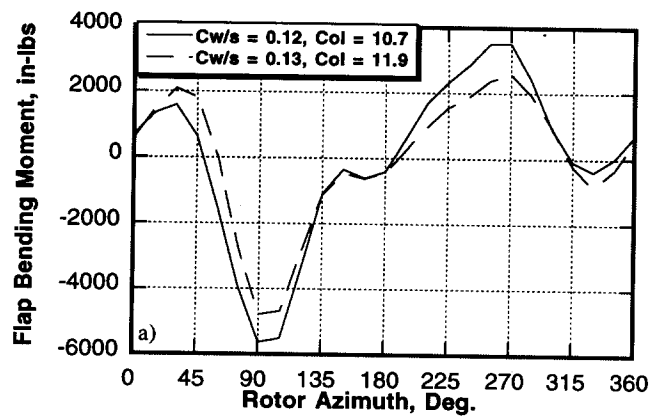


Figure 8. Calculated and measured flight test data for a,b) flap bending, $r/R = 0.30$, steady removed, c,d) pitch link load, steady removed, and e,f) blade section pitching moment, $r/R = 0.865$; trimmed to Cw/σ and one per rev flapping, counter 9017, $Cw/\sigma = 0.13, \mu = 0.23$.

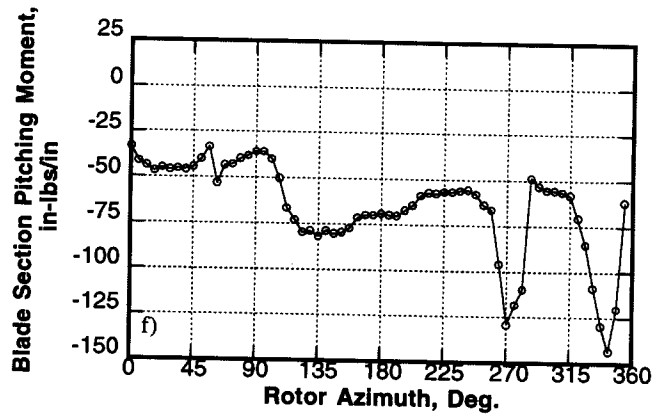
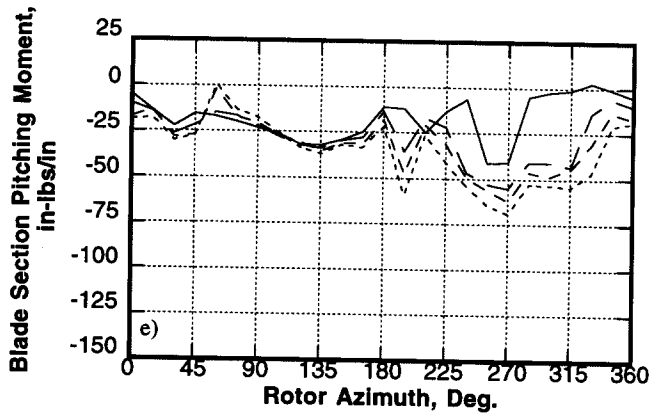
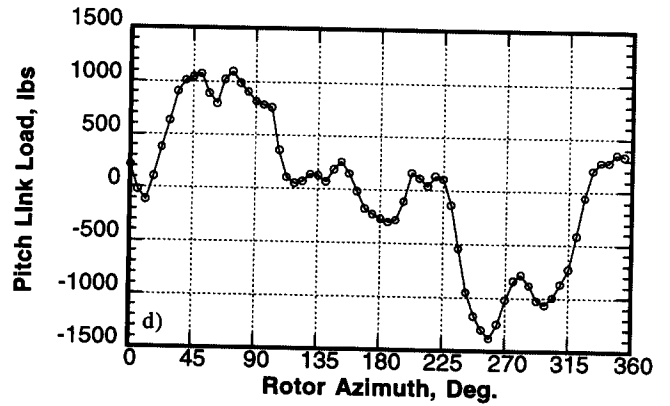
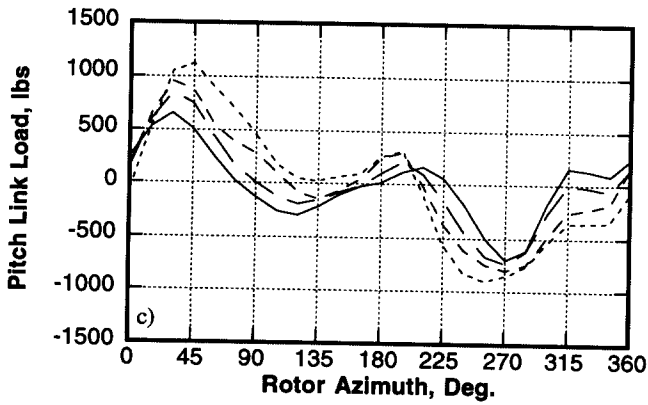
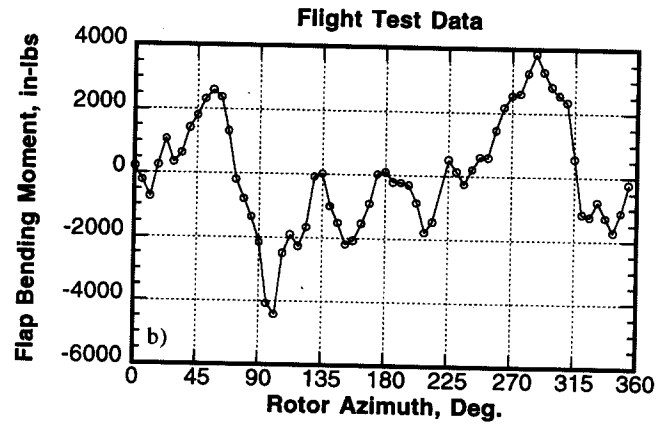
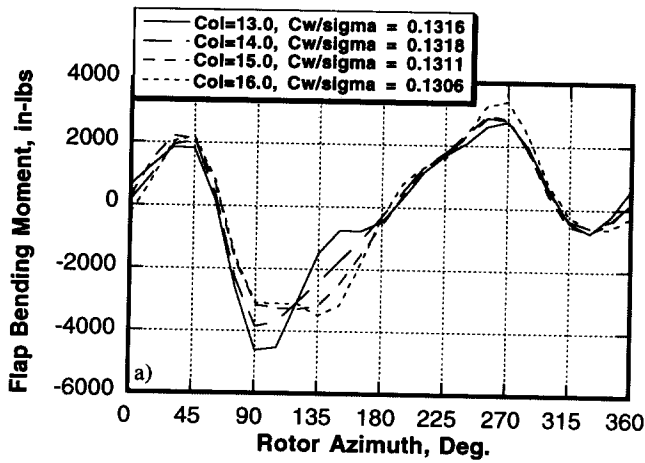


Figure 9. Calculated and measured flight test data for a,b) flap bending, $r/R = 0.30$, steady removed, c,d) pitch link load, steady removed, and e,f) blade section pitching moment, $r/R = 0.865$; trimmed to collective pitch and one per rev flapping, counter 9017, $C_w/\sigma = 0.13$, $\mu = 0.23$.

to the measured flapping. Predictions at different collective between 13° and 16° were made. These calculations are shown in Figure 9. These results still closely match the thrust level of the flight test condition as the rotor has reached its thrust limit and changes very little with increasing collective. The effects of increasing collective are an increase in loading for each parameter and the movement of the dynamic stall cycle forward from 255° to about 195° . There is also indication that a second dynamic cycle follows the first and that the airflow does not return to an unstalled state until late in the fourth quadrant.

After reviewing the above data it was determined that the calculations with a collective setting equal to 13° and trimmed to the measured flapping provided the best model to compare with different values of control system stiffness. The magnitude of the pitch link loading is closer to the flight value and the blade section pitching moment still shows the first major dynamic stall event occurring near 255° azimuth. Higher values of collective increase the pitch link loading closer to flight values, but make major changes to the initiation of the dynamic stall cycle.

Control Stiffness Variation

The stiffness value of the rotating (one spring) control system stiffness model was varied to study the calculated effects. The different values selected cover the range from 363 ft-lbs/deg, Ref. 6, to 1090 ft-lbs/deg, the measured reactionless mode stiffness. Two intermediate values of control system stiffness were also selected to match the two measured values of cyclic stiffness of 535 ft-lbs/deg. and 698 ft-lbs/deg. These values provide a relatively even increment over the given range to evaluate the effect.

Figure 10 shows the calculated blade pitch/torsion frequency at the nominal UH-60A rotor speed (258 rpm) as a function of the measured control system stiffness. The variation in blade pitch/torsion frequency was about 10% over the selected control system stiffness range.

Figure 11 shows the rotor response with the four different rotating control system stiffness values for the same trim condition, $\mu = 0.23$, collective = 13.0° compared with flight test data.

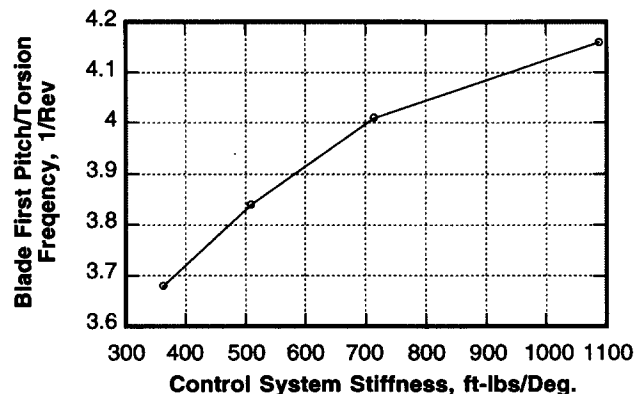


Figure 10. Calculated pitch/torsion mode frequencies at nominal rotor speed as a function of rotating control system stiffness, 258 rpm.

There was very little change in the flap bending moment calculation over the full range of control system stiffness values.

Since both pitch link load and the section pitching moment were strongly influenced by the blade torsional dynamics a bigger change was expected in these two parameters. This was true for pitch link load as Figure 11c shows that there was an improvement in predicting the pitch link oscillating load with the measured rotating control system stiffness value over the Ref. 6 value. There was about a 75% increase in half peak-to-peak pitch link loads from 400 lbs to 700 lbs over this control system stiffness range. Although the correlation for pitch link load was improved and the wave form was similar to the flight test data, this model was still far from matching the magnitude of the flight test data.

This improvement was also true for the section pitching moment as Figure 11e shows that with the Ref. 6 value of control system stiffness, the dynamic stall cycle near rotor azimuth 255° was completely absent. This suggests the need for an accurate control system stiffness to capture the correct dynamic stall characteristics when the dynamic loading and response of the blade pitch motion is close to the blade pitch/torsion frequency. Figure 11e also shows that for the rest of the azimuth the section pitching moment had very little variation for different values of control system stiffness. This suggests that an accurate control system stiffness was not needed to capture

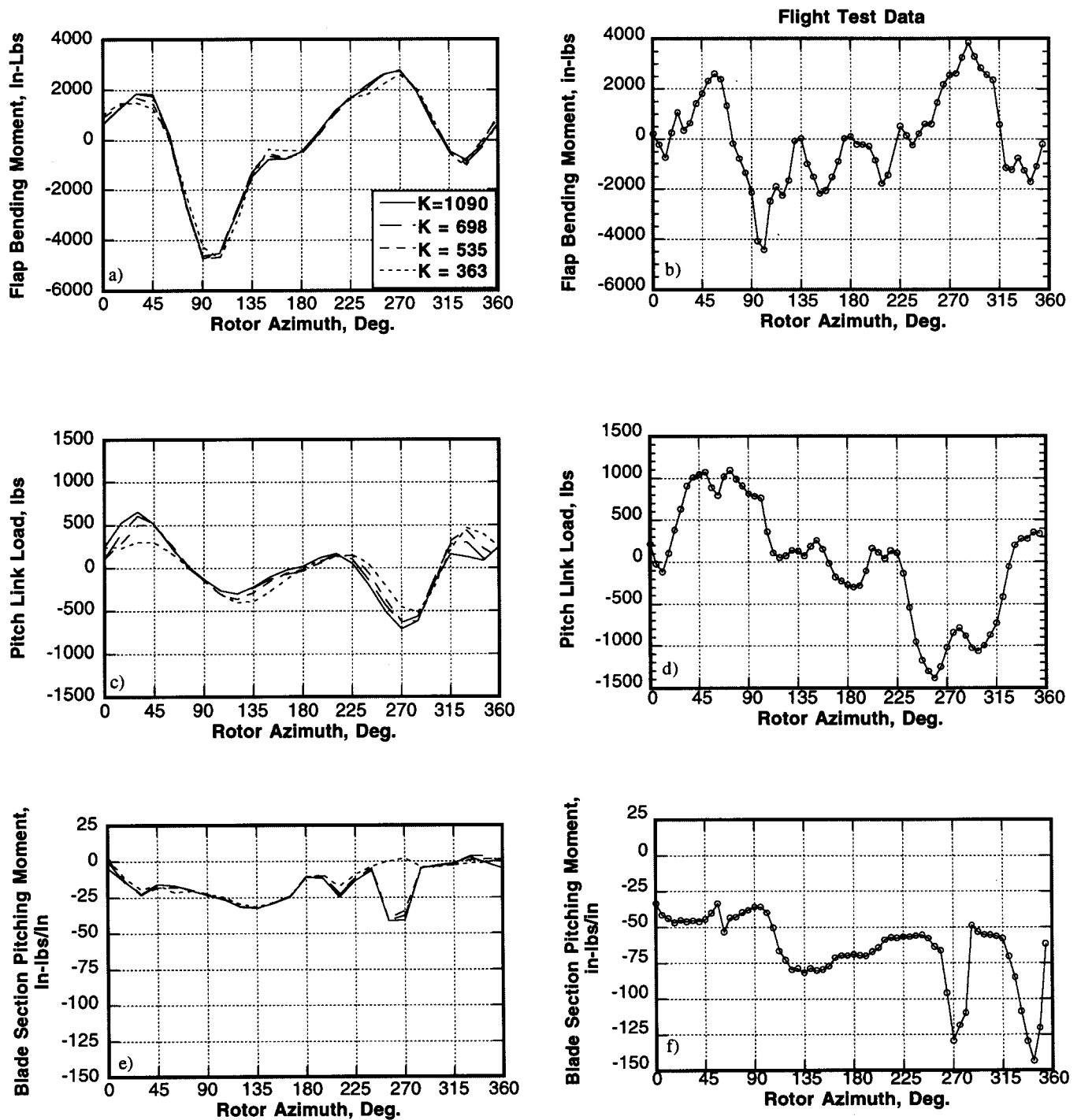


Figure 11. Calculated and measured flight test data of a,b) flap bending at $r/R = 0.30$, steady removed, c,d) pitch link load, steady removed, and e,f) blade section pitching moment, $r/R = 0.865$ as a function of rotor azimuth for different values of rotating control system stiffness, trimmed to collective = 13.0° and one per rev flapping, counter 9017, $C_w/\sigma = 0.13$, $\mu = 0.23$.

the aerodynamic characteristics when the dynamic loading and response of the blade pitch motion is removed from the pitch/torsion frequency. Finally, it should be noted that the overall value of the calculated section pitching moment was about half of the measured flight test value (Fig. 11f) for all conditions around the azimuth, not just the dynamic stall section. Since the blade structural model was validated with non-rotating shake test data and the control system stiffness has been measured the most likely source for this error would be the static and dynamic airfoil characteristics as well as three dimensional flow effects.

Figure 12 compares the rotor response between the rotating control system model and fixed system control system model using the correct measured stiffnesses.. There was very little change in value or wave form between the two models hinting that this model complexity was not required for this rotor loads flight condition. However, recall that the non-diagonal stiffness terms for the fixed system control system model are set to zero for these predictions. The full stiffness model for the fixed system control system model may provide different results.

Concluding Remarks

The control system stiffness of an UH-60A helicopter was measured for four different loading conditions. The measured results were then incorporated into the CAMRAD II comprehensive rotorcraft code. Calculations were performed with a variety of different control system stiffnesses and two different control system models to evaluate the sensitivity of rotor parameters to these changes.

1. The measured collective, cyclic, and reactionless control system stiffness of the UH-60A vary considerably from each other and are also higher than the value previously published in Ref. 6.
2. The azimuthal behavior of the measured stiffnesses is related to the swashplate and fixed system servo orientation.
3. Conversion of the individual stiffness measurements to the fixed system removes the azimuthal dependence.
4. The CAMRAD II analytical model shows qualitative agreement with the oscillatory rotor

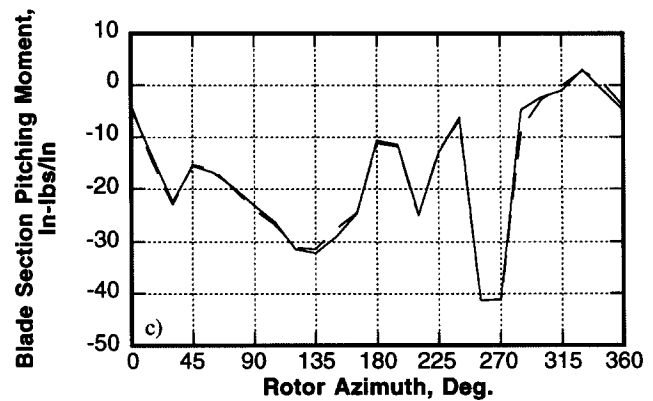
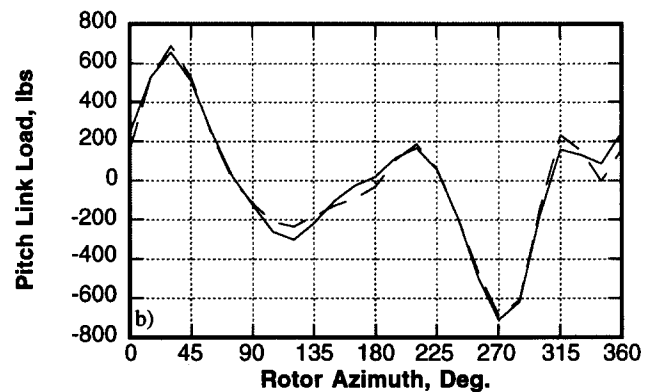
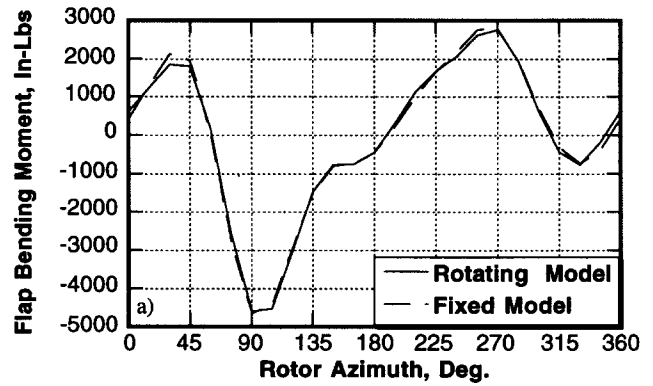


Figure 12. Calculated values of a) blade normal flapping at $r/R = 0.30$, b) pitch link load, and c) blade section pitching moment at $r/R = 0.865$ as a function of rotor azimuth for rotating and fixed models of control system stiffness, $C_w/\sigma = 0.13$, $\mu = 0.23$.

loads. The pitch link load correlation is best at highest collective, but the section pitching moment shows too much stall behavior in the fourth quadrant. The high frequency oscillation in flap bending and pitch link load are apparently not associated with stall, since these begin in the second quadrant of the disk.

5. The evaluation of the rotating control system model in CAMRAD II indicates that the measured value of control system stiffness improves pitch link load correlation over Ref. 6.

6. An accurate control system stiffness is needed to accurately capture the dynamic stall characteristics. Smaller, though incorrect, values of control system stiffness can, at times, adequately characterize normal flight condition loads without dynamic stall.

7. Measurements of the control system stiffness and correlation with non-rotating shake test of blade models narrows the range of possibilities for source of differences between measurements and calculations. A study of the static and dynamic airfoil characteristics in three dimensional flow should be considered.

8. The fixed control system model is not required to improve prediction of dynamic stall as both the rotating and fixed system control system models show the same rotor response.

References

1. Bousman, W.G., "A Qualitative Examination of Dynamic Stall from Flight Test Data," American Helicopter Society 53rd Annual Forum, Virginia Beach, Virginia, April 29-May 1 1997.
2. Kufeld, R.M., Balough, D.L., Cross, J.L., Studebaker, K.F., Jennison, C.D., and Bousman, W.G., "Flight Testing of the UH-60A Airloads Aircraft," 50th Annual American Helicopter Society Forum, Washington, DC, May 1994.
3. Johnson, W., "Technology Drivers in the Development of CAMRAD II," American Helicopter Society, Aeromechanics Specialists Meeting, San Francisco, California, January 1994.
4. Johnson, W., "Rotorcraft Aerodynamics Models for a Comprehensive Analysis," American Helicopter Society 54th Annual Forum Proceedings, Washington, DC, May 20-22 1998..
5. Hamade, K.S. and Kufeld, R.M. "Modal Analysis of UH-60A Instrumented Rotor Blades," NASA TM 4239, November 1990.
6. Shanley, J.P., "Application of the Comprehensive Analytical Model of Rotorcraft Aerodynamics and Dynamics to the UH-60A Aircraft," SER-72126, February 1986.
7. Johnson, W. Helicopter Theory, Princeton University Press, Princeton, New Jersey, 1980.
8. Bousman, W.G. and Maier, T.H., "An Investigation of Helicopter Rotor Blade Flap Vibratory Loads," American Helicopter Society 48th Annual Forum, Washington, DC, June 1992.
9. Lim, J.W., "Analytical Investigation of UH-60A Flight Blade Airloads and Loads Data," American Helicopter Society 51th Annual Forum Proceedings, Fort Worth, Texas, May 9-11 1995.
10. Leishman, J.G., and Beddoes, T.S. "A Semi-Empirical Model for Dynamic Stall" Journal of the American Helicopter Society, Volume 24, Number 3, July 1989.